Nonlinear Time-Averaged Model in Surf and Swash Zones

Bradley D. Johnson[1] and Nobuhisa Kobayashi, Member, ASCE[2]

Abstract

A time-averaged model is developed to predict the cross-shore variations of the mean and standard deviation of the free surface elevation from outside the surf zone to the lower swash zone on beaches. This new model includes nonlinear correction terms in the cross-shore radiation stress and energy flux that become important in very shallow water. Empirical formulas are proposed for the skewness and kurtosis as well as the ratio of the root-mean-square wave height to the mean water depth which increases rapidly near the still water shoreline. The developed model is shown to be in agreement with three irregular wave tests on a 1:16 smooth impermeable slope and two tests of quasi-equilibrium terraced and barred beaches. The model can predict the observed large increase of wave setup near the still water shoreline. The developed model and empirical formulas will need to be verified using additional experiments.

Introduction

The need for a simple model for the wave motion in the swash zone on a beach has been pointed out in relation to the prediction of beach erosion and recovery near the shoreline [e.g., Hedegaard et al. (1992)]. The time-dependent numerical model based on the finite-amplitude shallow-water equations (Kobayashi and Wurjanto 1992) has been shown to be capable of predicting the swash characteristics on natural beaches (Raubenheimer et al. 1995; Raubenheimer and Guza 1996). However, the time-dependent numerical model requires significant computation time and is hard to incorporate in beach profile models. The time-averaged models for random waves represented by the root-mean-square wave height [e.g., Battjes and Janssen (1978)] or expressed as the superposition of regular waves [e.g., Dally (1992)] are much more efficient computationally but do not predict the wave conditions in the swash zone (Cox et al. 1994).

A nonlinear time-averaged model is developed here to predict the cross-shore variations of the wave setup, $\overline{\eta}$, and the root-mean-square wave height, H_{rms}, from outside the surf zone to the lower swash zone where H_{rms} is defined as $H_{rms} = \sqrt{8}\,\sigma$ with σ

---

[1]Ph.D. Student, Dept. of Civ. & Envir. Engrg., Univ. of Delaware, Newark, DE 19716, USA
[2]Professor & Assoc. Director, Center for Applied Coastal Research, University of Delaware, Newark, DE 19716.

= standard deviation of the free surface elevation. This model is based on the time-averaged continuity, momentum, and energy equations derived by time-averaging the nonlinear equations used in the time-dependent model of Kobayashi and Wurjanto (1992). The time-averaged equations can be solved numerically with much less computation time but require empirical relationships to close the problem. The time-averaged rate of energy dissipation due to random wave breaking is estimated by modifying the empirical formula of Battjes and Stive (1985) to account for the landward increase of $H_{rms}/\overline{h}$ near the shoreline where $\overline{h}$ = mean water depth. The skewness s and the kurtosis K of the free surface elevation included in the time-averaged momentum and energy equations are expressed empirically as a function of $H_{rms}/\overline{h}$.

The developed model is compared with three tests conducted on a 1:16 smooth impermeable slope and two tests on quasi-equilibrium terraced and barred beaches consisting of fine sand. This new time-averaged model is shown to be capable of predicting the cross-shore variations of $\overline{\eta}$ and H_{rms} of the free surface elevation from outside the surf zone to the lower swash zone of frequent wave uprush and downrush. The model of Battjes and Stive (1985) considerably underpredicts $\overline{\eta}$ and H_{rms} near the still water shoreline. The new model will need to be verified using additional experiments because the empirical formulas adopted in the model are developed using the same five tests.

New Time-Averaged Model

The assumptions of alongshore uniformity and normally incident irregular waves are made in the following. To account for nonlinear effects in very shallow water, use is made of the time-averaged equations derived from the finite-amplitude shallow-water equations. Assuming that the beach is impermeable, the time-averaged continuity equation with the overbar denoting time-averaging is expressed as

$$\overline{hU} = 0 \tag{1}$$

where h = instantaneous water depth; and U = instantaneous depth-averaged horizontal velocity. The time-averaged cross-shore momentum equation is written as (Kobayashi et al. 1989)

$$\frac{dS_{xx}}{dx} = -\rho g\overline{h} \, \frac{d\overline{\eta}}{dx} \tag{2}$$

with

$$S_{xx} = \rho \left[\overline{hU^2} + \frac{1}{2}g\overline{(\eta - \overline{\eta})^2} \right] \tag{3}$$

in which x = cross-shore coordinate taken to be positive landward; S_{xx} = cross-shore radiation stress; ρ = fluid density; g = gravitational acceleration; and η = instantaneous free surface elevation above the still water level (SWL). The time-averaged bottom shear stress may be neglected in (2) as explained by Kobayashi and Johnson (1998). The bottom elevation z_b given by $z_b = (\eta - h)$ is assumed to depend on x only. The time-averaged energy equation corresponding to (1) and (2) may be expressed as (Kobayashi and Wurjanto 1992)

$$\frac{d}{dx} \left(\overline{E_F} \right) = -\overline{D_B} \tag{4}$$

with

$$\overline{E_F} = \frac{1}{2} \rho \ \overline{hU^3} + \rho g \overline{\eta hU} \tag{5}$$

in which $\overline{E_F}$ = energy flux per unit width; and $\overline{D_B}$ = energy dissipation rate due to wave breaking which needs to be estimated empirically in this time-averaged model.

To simplify (1), (2), and (4), the instantaneous free surface elevation η is expressed as

$$\eta = \overline{\eta} + \sigma \eta_* \tag{6}$$

where $\overline{\eta}$ and σ = mean and standard deviation of η; and η_* = normalized free surface elevation with $\overline{\eta_*} = 0$ and $\overline{\eta_*^2} = 1$. If wave reflection is negligible, linear long wave theory may be used locally to relate the oscillatory components $(\eta - \overline{\eta})$ and $(U - \overline{U})$ inside and outside the surf zone (Guza and Thornton 1980; Kobayashi et al. 1998). This relationship together with (6) yields

$$U = \overline{U} + \sqrt{\frac{g}{\overline{h}}} \ \sigma \eta_* \tag{7}$$

Eq. (7) is necessary to reduce the number of unknown variables in the time-averaged model although the local reflection coefficient may not be small near the still water shoreline on beaches (Baquerizo et al. 1997). Substitution of (6) and (7) into (1) with $h = (\eta - z_b)$ and $\overline{h} = (\overline{\eta} - z_b)$ yields

$$\overline{U} = -\sigma_*^2 \sqrt{g\overline{h}} \quad ; \quad \sigma_* = \frac{\sigma}{\overline{h}} \tag{8}$$

which indicates that $\overline{U}$ is negative and represents return current (Kobayashi et al. 1989). Although (8) does not account for the landward mass flux due to a surface roller, it predicted the undertow measured at the mid-depth below SWL fairly accurately (Kobayashi et al. 1997, 1998).

Substitution of (6) and (7) with (8) into (3) yields

$$S_{xx} = \frac{1}{8} \ \rho \ g \ H_{rms}^2 \left[\left(2n - \frac{1}{2}\right) + C_s\right] \quad ; \quad H_{rms} = \sqrt{8} \ \sigma \tag{9}$$

with

$$C_s = \sigma_* s - \sigma_*^2 \tag{10}$$

where s = skewness of η and η_* with $\overline{\eta_*^3} = s$; n = finite-depth adjustment parameter with $n = 1$ in shallow water; and C_s = nonlinear correction term for S_{xx}. For linear progressive waves in finite depth, n is normally expressed as [e.g., Battjes and Stive (1985)]

$$n = \frac{1}{2} \left[1 + \frac{2k_p \overline{h}}{\sinh\left(2k_p \overline{h}\right)}\right] \tag{11}$$

where k_p = linear wave number corresponding to the spectral peak period T_p outside the surf zone. The cross-shore variation of T_p may be neglected in (11) because $n = 1$ in shallow water for any reasonable representative wave period used to calculate k_p. The cross-shore radiation stress S_{xx} based on linear wave theory is given by (9) with

$C_s = 0$. C_s is on the order of unity near the still water shoreline and can not be neglected in the swash zone (Kobayashi and Johnson 1998).

Substitution of (6) and (7) with (8) into (5) yields

$$\overline{E}_F = \frac{1}{8} \rho g H_{rms}^2 n C_p (1 + C_F) \tag{12}$$

with

$$C_F = \frac{3}{2} s \sigma_* \left(1 - \sigma_*^2\right) + \frac{1}{2} \sigma_*^2 (K - 5) + \sigma_*^4 \tag{13}$$

where C_p = phase velocity based on T_p with $C_p = \sqrt{g\overline{h}}$ in shallow water; C_F = nonlinear correction term for $\overline{E}_F$; and K = kurtosis of η and η_* with $\overline{\eta_*^4} = K$. The finite-depth adjustment is included in (12) in the same way as (9) where $n C_p$ in (12) is the group velocity based on T_p. The cross-shore energy flux $\overline{E}_F$ based on linear wave theory is given by (12) with $C_F = 0$ where C_F is on the order of unity near the still water shoreline (Kobayashi and Johnson 1998).

The momentum equation (2) with (9) and the energy equation (4) with (12) need to be solved numerically to predict the cross-shore variations of the wave setup $\overline{\eta} = (\overline{h} + z_b)$ and the root-mean-square wave height $H_{rms} = \sqrt{8} \sigma$. These equations reduce to those used in the existing time-averaged models [e.g., Battjes and Stive (1985)] if $C_s = 0$ and $C_F = 0$. To estimate the nonlinear correction terms C_s and C_F using (10) and (13) with $\sigma_* = \sigma/\overline{h}$, the skewness s and the kurtosis K are assumed to be expressed in the following empirical forms

$$s = f_s \left(H_{rms}/\overline{h}\right) \qquad ; \qquad K = f_K(s) \tag{14}$$

where f_s and f_K = empirical functions which will be obtained using the five tests discussed later.

Finally, the energy dissipation rate $\overline{D}_B$ due to wave breaking in the energy equation (4) needs to be estimated. The empirical formula proposed by Battjes and Janssen (1978) and calibrated by Battjes and Stive (1985) is adopted here for its simplicity. The formula proposed by Thornton and Guza (1983) may predict the distributions of breaking and nonbreaking wave heights more accurately but requires additional empirical parameters. In the present formulation, the exponential gamma function may be used to describe the probability density function of η instead of wave heights after the cross-shore variations of $\overline{\eta}$, σ, and s are predicted (Kobayashi et al. 1997, 1998).

The calibrated formula by Battjes and Stive (1985) is given by

$$\overline{D_B} = \frac{\alpha}{4} \rho g f_p Q H_m^2 \tag{15}$$

with

$$\frac{Q - 1}{\ln Q} = \left(\frac{H_{rms}}{H_m}\right)^2 \tag{16}$$

$$H_m = \frac{0.88}{k_p} \tanh\left(\frac{\gamma\, k_p\, \overline{h}}{0.88}\right) \tag{17}$$

$$\gamma = 0.5 + 0.4\tanh\left(33\,\frac{H_{rmso}}{L_o}\right) \quad ; \quad L_o = \frac{g\, T_p^2}{2\pi} \tag{18}$$

where α = empirical coefficient recommended as $\alpha = 1$; f_p = spectral peak frequency given by $f_p = T_p^{-1}$; Q = local fraction of breaking waves in the range $0 \le Q \le 1$; H_m = local depth-limited wave height; k_p = linear wave number calculated using f_p and $\overline{h}$; γ = empirical parameter determining $H_m = \gamma\overline{h}$ in shallow water; L_o = deep-water wavelength based on T_p; and H_{rmso} = deep-water value of H_{rms} calculated using linear wave shoaling theory with T_p, $\overline{h}$ and H_{rms} specified at the seaward boundary of the numerical model.

The empirical parameter γ is uncertain in light of the field data by Raubenheimer et al. (1996) but is estimated using (18) without any additional calibration. Relatedly, Battjes and Janssen (1978) indicated that $\overline{D}_B$ given by (15) would underestimate the actual energy dissipation rate and produce $H_{rms} > H_m$ near the shoreline, although (16) with $Q \le 1$ requires $H_{rms} \le H_m$. They recommended use of a cutoff of $H_{rms} = H_m$ when $H_{rms} > H_m$. This adjustment leads to $H_{rms} = \gamma\overline{h}$ near the shoreline. However, $H_{rms}/\overline{h}$ is not constant and increases landward where $H_{rms}/\overline{h} \simeq 2$ at the still water shoreline for the SUPERTANK data of Kriebel (1994). As a result, (15) with (16)–(18) is assumed to be valid only in the outer zone $x < x_i$ with x_i = cross-shore location where Q computed by (16) becomes unity and the still water depth decreases landward in the region $x > x_i$. The latter condition is required for a barred beach to allow $Q < 1$ landward of the bar crest where $Q = 1$ may occur. For the inner zone $x > x_i$, the ratio $H_* = H_{rms}/\overline{h}$ is assumed to be expressed as

$$H_* = \gamma + (\gamma_s - \gamma)\, x_*^{\beta} \quad ; \quad x_* = \frac{x - x_i}{x_s - x_i} > 0 \tag{19}$$

where γ_s = value of H_* on the order of two at the still water shoreline located at $x = x_s$; and β = empirical parameter. The values of γ_s and β will be calibrated using the five tests discussed later. Eq. (19) describes the landward increase of H_* from $H_* = \gamma$ at $x = x_i$ to $H_* = \gamma_s$ at $x = x_s > x_i$. For the inner zone $x > x_i$, the momentum equation (2) and (19) are used to predict the cross-shore variations of $\overline{h}$ and H_{rms}, whereas the energy equation (4) is used to estimate $\overline{D}_B$ which must be positive or zero.

The numerical model called CSHORE (Kobayashi and Johnson 1998) is developed to solve (2) and (4) with (9)–(19) where CSHORE includes the option to include the bottom friction effects neglected in (2) and (4). The seaward boundary of CSHORE is located at $x = 0$ where the values of T_p, H_{rms} and $\overline{\eta}$ at $x = 0$ are specified as input. The bottom elevation $z_b(x)$ in the region $x \ge 0$ is also specified as input and the location x_s of the still water shoreline is found using $z_b(x = x_s) = 0$. First-order finite-difference approximations of (2) and (4) are expressed as

$$\overline{\eta}_{j+1} = \overline{\eta}_j - \left[\rho\, g\left(\overline{h}_{j+1} + \overline{h}_j\right)\right]^{-1} \left\{2\left[(S_{xx})_{j+1} - (S_{xx})_j\right]\right\} \tag{20}$$

$$\left(\overline{E}_F\right)_{j+1} = \left(\overline{E}_F\right)_j - \frac{\Delta x}{2}\left[\left(\overline{D}_B\right)_{j+1} + \left(\overline{D}_B\right)_j\right] \tag{21}$$

where the subscripts $(j + 1)$ and j indicate the quantities at nodes located at x_{j+1} and x_j, respectively, with $\Delta x = (x_{j+1} - x_j)$ being the nodal spacing. In the subsequent computations for the laboratory data, use is made of $\Delta x \simeq 10$ cm. For the known quantities at node j, the unknown quantities at node $(j + 1)$ are computed by solving (20) and (21) using an iteration method starting from σ^2_{j+1} computed using (21) with $(\overline{D}_B)_{j+1} = (\overline{D}_B)_j$. The adopted iteration method is found to converge within several iterations. The convergency is based on the differences between the iterated values of σ_{j+1} and $\overline{h}_{j+1}$ being less than the specified small value ϵ, where $\epsilon = 0.01$ mm is used in the subsequent computations. If $Q_{j+1} = 1$ and $(dz_b/dx) > 0$ for $x \geq x_{j+1}$, the inner zone is reached and $x_i = x_{j+1}$ is set.

For the nodes located in the inner zone $x > x_i$, (19) is used to obtain $H_* = H_{rms}/\overline{h}$ and $\sigma_* = H_*/\sqrt{8}$. Since the mean water depth $\overline{h}$ can become very small in the inner zone, (2) with (9) is rewritten as

$$(2P + 1)\frac{d\overline{h}}{dx} = -\overline{h}\frac{dP}{dx} - \frac{dz_b}{dx} \quad \text{for} \quad x > x_i \tag{22}$$

with

$$P = \sigma^2_* \left[\left(2n - \frac{1}{2}\right) + \sigma_* s - \sigma^2_*\right] \tag{23}$$

A first-order finite difference approximation of (22) between nodes j and $(j + 1)$ yields

$$\overline{h}_{j+1} = (3P_{j+1} + P_j + 2)^{-1} \left\{(P_{j+1} + 3P_j + 2)\overline{h}_j - 2\left[(z_b)_{j+1} - (z_b)_j\right]\right\} \tag{24}$$

Eq. (24) is solved using an iteration method starting from the value of n_{j+1} involved in P_{j+1} calculated using $\overline{h}_j$ where $(\sigma_*)_{j+1}$ and s_{j+1} are known using (19) and (14), respectively. Since n given by (11) is essentially unity in shallow water, this interaction method converges rapidly. After $\overline{h}_{j+1}$ is computed, the energy equation (4) is used to obtain $(\overline{D}_B)_{j+1}$. The computation is marched landward until $\overline{h}_{j+1} < \epsilon$.

EXPERIMENTS AND EMPIRICAL FORMULAS

Two different experiments were conducted in a wave tank that was 30 m long, 2.4 m wide, and 1.5 m high. These experiments were explained in detail by Kobayashi et al. (1997, 1998). Irregular waves based on the TMA spectrum were generated with a piston-type wave paddle. Three tests were conducted with a plywood beach of a 1:16 slope. The water depth in the tank was 76.2 cm. For each test, 17 runs were performed to measure free surface elevations using eight capacitance wave gages. Wave gages partially immersed in gage wells were used for the free surface measurements near the still water shoreline. In addition, two tests were conducted with a fine sand beach whose initial slope was 1:12. The sand was well-sorted and its median diameter was 0.18 mm. These two tests with specified random waves were conducted after the sand beach was exposed to the specified wave action for several days and became quasi-equilibrium with the bottom elevation changes less than about 1 cm/hr. For each of the two tests, 21 runs were performed to measure free surface elevations using ten wave gages. Wave gages near the still water shoreline were partially buried in the sand. The duration of each run in these five tests was 400 s and the initial transient duration of 75 s was removed. The sampling rate was 20 Hz.

Table 1: Wave Conditions at Seaward Boundary and Breaker Parameter γ for Five Tests

Test (1)	d (cm) (2)	$\overline{\eta}$ (cm) (3)	T_p (s) (4)	H_{rms} (cm) (5)	H_{inc} (cm) (6)	R (7)	γ (8)	x_i (m) (9)	x_s (m) (10)
1	75.0	0.03	1.5	12.4	12.2	0.14	0.84	11.1	12.0
2	75.0	-0.32	2.8	16.9	15.8	0.15	0.67	9.0	12.0
3	76.2	-0.24	4.7	18.4	18.4	0.17	0.56	8.3	13.0
4	60.0	-0.15	1.6	12.8	12.9	0.19	0.83	13.3	13.8
5	60.0	-0.12	2.8	14.6	14.3	0.25	0.65	12.4	13.7

Table 1 lists the wave conditions at the seaward boundary located at $x = 0$ for each of the five tests where $d =$ still water depth; $\overline{\eta} =$ wave setup or set-down; $T_p =$ spectral peak period; and $H_{rms} =$ root-mean-square wave height defined as $H_{rms} = \sqrt{8}\,\sigma$ with $\sigma =$ standard deviation of the measured free surface oscillation. Tests 1, 2 and 3 are the 1:16 slope tests described by Kobayashi et al. (1998), whereas tests 4 and 5 correspond to the sand beach tests explained by Kobayashi et al. (1997). The wave setup or set-down is very small at $x = 0$ outside the surf zone. The measured wave conditions at $x = 0$ include the slight effects of reflected waves. The incident and reflected waves at $x = 0$ were estimated using a three-gage method by Kobayashi et al. (1997, 1998). Table 1 lists the estimated values of the spectral root-mean-square wave height, $H_{inc} = \sqrt{8m_{oi}}$, with $m_{oi} =$ zero-moment of the incident wave spectrum at $x = 0$, and the average reflection coefficient, $R = \sqrt{m_{or}/m_{oi}}$, with $m_{or} =$ zero-moment of the reflected wave spectrum at $x = 0$. The difference between H_{rms} and H_{inc} is negligible except for test 2 with $(H_{rms} - H_{inc})/H_{rms} = 0.065$. The reflection coefficient was in the narrow range $0.14 \leq R \leq 0.25$ and slightly larger for tests 4 and 5 with the foreshore slope of about 1:5 at the still water shoreline.

The measured values of $\overline{\eta}$, T_p, and H_{rms} at $x = 0$ listed in Table 1 are specified as input to CSHORE. The measured bottom elevation $z_b(x)$ in the region $x \geq 0$ is also specified as input where Table 1 lists the cross-shore location x_s of the still water shoreline for each test. The bottom profile $z_b(x)$ will be presented in conjunction with the measured and predicted cross-shore variations of $\overline{\eta}$ and H_{rms}. The breaker parameter γ calculated using (18) and the cross-shore location x_i at the seaward limit of the inner zone computed by CSHORE are listed in Table 1.

The measured values of $H_* = H_{rms}/\overline{h}$ in the inner zone $x > x_i$ are used to calibrate the new empirical parameters γ_s and β in (19) for the five tests. Fig. 1 shows the
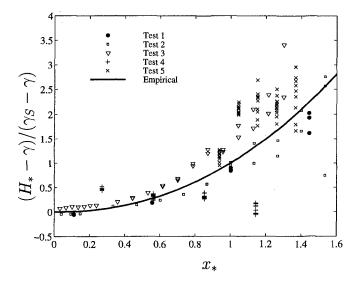
Figure 1: Empirical Formula for $H_* = H_{rms}/\overline{h}$ in Inner Zone $x > x_i$.

measured values of $(H_* - \gamma)/(\gamma_s - \gamma)$ with $\gamma_s = 2$ as a function of $x_* = (x - x_i)/(x_s - x_i)$ where the values of γ, x_i, and x_s for each test are listed in Table 1. The trend of the scattered data points for the five tests may be represented by (19) with $\gamma_s = 2$ and $\beta = 2.2$. Fig. 1 shows that H_* increases gradually from $H_* = \gamma$ at $x_* = 0$ and more rapidly above the still water shoreline located at $x_* = 1$. It is noted that the large scatter in the region $x_* > 1$ is caused partly by the scatter of data points obtained in repeated runs due to the difficulty in measuring $\overline{h}$ and H_{rms} accurately in the swash zone.

The measured values of H_*, s, and K in the entire region $x \geq 0$ for the five tests are analyzed to obtain the empirical relationships expressed by (14). Fig. 2 shows the skewness s as a function of $H_* = H_{rms}/\overline{h}$. The trend of the scattered data points in Fig. 2 are simply represented by three straight lines

$$
\begin{aligned}
s &= 2H_* && \text{for} \quad 0.1 < H_* \leq 0.5 \\
s &= 1.5 - H_* && \text{for} \quad 0.5 \leq H_* \leq 1.0 \\
s &= 0.7H_* - 0.2 && \text{for} \quad 1.0 \leq H_* \lesssim 5
\end{aligned}
\tag{25}
$$

The skewness s increases initially with the increase of H_* due to wave shoaling but decreases after wave breaking. Both s and H_* increase rapidly near and beyond the still water shoreline. Fig. 3 shows the relationship between the kurtosis K and the skewness s which may be expressed as

$$
K = 3 + s^{2.2} \qquad \text{for} \quad 0.2 < s \lesssim 3
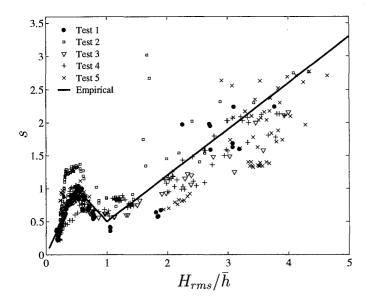\tag{26}
$$

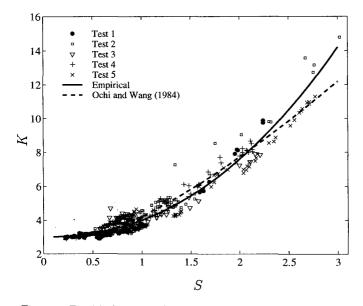Figure 2: Empirical Formula for Skewness s as a Function of H_*.

Figure 3: Empirical Formula for Kurtosis K as a Function of Skewness s.

The empirical relationship between K and s proposed by Ochi and Wang (1984) yields similar agreement as shown in Fig. 3. However, their expression is more complicated and (26) is adopted here for its simplicity.

COMPARISONS WITH FIVE TESTS

The numerical model CSHORE is compared with the five tests listed in Table 1 and used to develop the empirical formulas (25) and (26) as well as (19) with $\gamma_s = 2$ and $\beta = 2.2$. Figs. 4–8 compare the measured and computed cross-shore variations of $\overline{\eta}$ and H_{rms} for tests 1–5, respectively. The variations of $\overline{\eta}$ and H_{rms} computed by the model of Battjes and Stive (BJS hereafter) are also plotted in these figures. The bottom elevation $z_b(x)$ above and below SWL is shown in the first and second panels, respectively, in Figs. 4–8 to show the effects of the beach profile on the wave setup $\overline{\eta}$ and the root-mean-square wave height H_{rms}. The data points from repeated runs in each test are presented without averaging to indicate the degree of the data scatter which was apparent in the swash zone because of the difficulty in measuring small water depth accurately (Kobayashi et al. 1997, 1998).

For tests 1–3 shown in Figs. 4–6, breaker types on the 1:16 smooth slope varied from mostly spilling breakers for test 1 to predominantly plunging breakers for test 3. Correspondingly, the inner zone became wider from test 1 to test 3 where $(x_s - x_i)$ = 0.9, 3.0 and 4.7 m for tests 1, 2, and 3, respectively, in Table 1. Comparing CSHORE and the BJS model, the computed variations of $\overline{\eta}$ and H_{rms} in the outer zone $x < x_i$ are practically the same in view of the larger uncertainty associated with the empirical formula (15) with (16)–(18). No attempt is made to calibrate γ to improve the agreement for H_{rms} in the outer zone for test 2. In the inner zone $x > x_i$, CSHORE is capable of predicting the larger increase of the wave setup $\overline{\eta}$ and the more gradual decrease of the wave height H_{rms} in the inner zone.

For tests 4 and 5 shown in Figs. 7 and 8, incident waves shoaled and broke on the small bar at the edge of the terrace. Plunging breakers at the terrace edge were intense in test 5. Wave breaking was reduced on the terrace before incident waves broke again in the swash zone. The BJS model is capable of predicting this wave transformation across the terrace except for the detailed variations of H_{rms} at the terrace edge. The differences between CSHORE and BJS model are limited essentially in the narrow inner zone where $(x_s - x_i) = 0.5$ and 1.3 m for tests 4 and 5, respectively, in Table 1. CSHORE allows the extension of BJS model into the lower swash zone.

CONCLUSIONS

A time-averaged model is developed to predict the cross-shore variations of the mean and standard deviation of the free surface elevation from outside the surf zone to the lower swash zone. This time-averaged model derived from the time-dependent continuity, momentum, and energy equations which were used successfully to predict irregular wave runup on beaches includes nonlinear corrections terms in the cross-shore radiation stress and energy flux. The correction terms involving the skewness and kurtosis are important in very shallow water. The time-averaging of the time-dependent equations reduces computation time considerably but creates a closure problem. The energy dissipation rate due to wave breaking is estimated using an
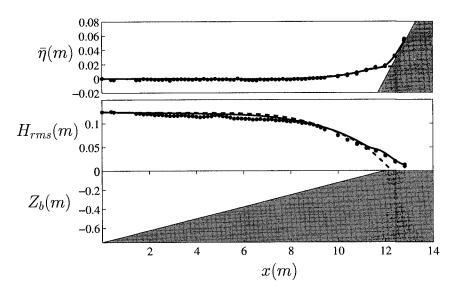
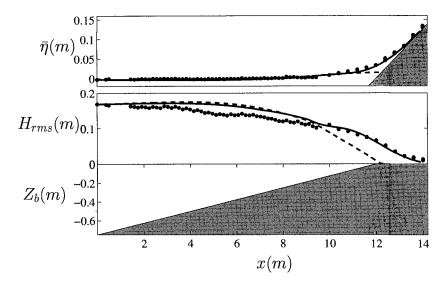Figure 4: Measured and Computed Setup $\bar{\eta}$, and Height H_{rms} for Test 1.

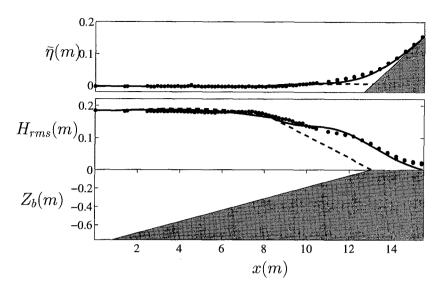Figure 5: Measured and Computed Setup $\bar{\eta}$, and Height H_{rms} for Test 2.

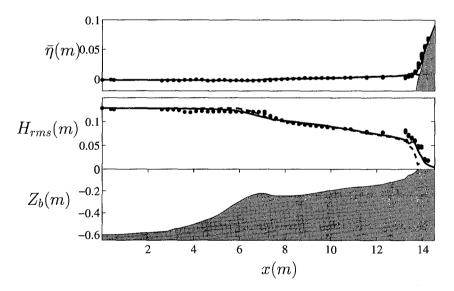Figure 6: Measured and Computed Setup $\bar{\eta}$, and Height H_{rms} for Test 3.

Figure 7: Measured and Computed Setup $\bar{\eta}$, and Height H_{rms} for Test 4.
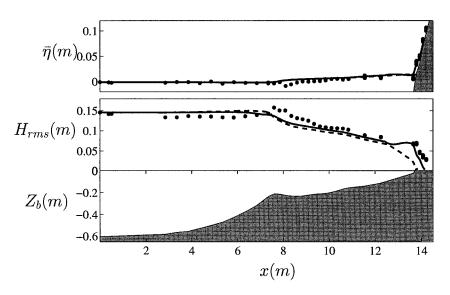
Figure 8: Measured and Computed Setup $\bar{\eta}$, and Height H_{rms} for Test 5.

existing empirical formula in the outer zone. In the inner zone near the still water shoreline, a new empirical formula for $H_* = H_{rms}/\bar{h}$ is proposed to describe the landward increase of H_*. In addition, simple empirical formulas are proposed to express the skewness and kurtosis as a function of H_*.

The developed model is compared with three irregular wave tests on a 1:16 smooth impermeable slope and two tests on quasi-equilibrium terraced and barred beaches. The major improvements of the new model in comparison to existing models are that it is capable of predicting the wave setup and root-mean-square wave height near the still water shoreline. Since the new empirical formulas are developed using the same five tests, the new model will need to be verified using additional tests. Coupling of the new wave model with a cross-shore sediment transport model may make it feasible to predict the erosion and recovery near the still water shoreline.

ACKNOWLEDGMENT

APPENDIX. REFERENCES

Baquerizo, A., Losada, M.A., Smith, J.M., and Kobayashi, N. (1997). "Cross-shore

variation of wave reflection from beaches." *J. Wtrwy., Port, Coast. and Oc. Engrg.*, ASCE, 123(5), 274–279.

Battjes, J.A., and Janssen, J.P.F.M. (1978). "Energy loss and set-up due to breaking of random waves." *Proc., 16th Coast. Engrg. Conf.*, ASCE, New York, N.Y., 1, 569–587.

Battjes, J.A., and Stive, M.J.F. (1985). "Calibration and verification of a dissipation model for random breaking waves." *J. Geophys. Res.*, 90(C5), 9159–9167.

Cox, D.T., Kobayashi, N., and Kriebel, D.L. (1994). "Numerical model verification using SUPERTANK data in surf and swash zones." *Proc., Coast. Dynamics '94*, ASCE, New York, N.Y., 248–262.

Dally, W.R. (1992). "Random breaking waves: Field verification of a wave-by-wave algorithm for engineering application." *Coast. Engrg.*, 16, 369–397.

Guza, R.T., and Thornton, E.B. (1980). "Local and shoaled comparisons of sea surface elevations, pressures, and velocities." *J. Geophys. Res.*, 85(C3), 1524–1530.

Hedegaard, I.B., Roelvink, J.A., Southgate, H., Pechon, P., Nicholson, J., and Hamm, L. (1992). "Intercomparison of coastal profile models." *Proc., 23rd Coast. Engrg. Conf.*, ASCE, New York, N.Y., 2, 2108–2121.

Kobayashi, N., DeSilva, G.S., and Watson, K.D. (1989). "Wave transformation and swash oscillation on gentle and steep slopes." *J. Geophys. Res.*, 94(C1), 951–966.

Kobayashi, N., Herrman, M.N., Johnson, B.D., and Orzech, M.D. (1998). "Probability distribution of surface elevation in surf and swash zones." *J. Wtrwy., Port, Coast. and Oc. Engrg.*, ASCE, 124(3), 99–107.

Kobayashi, N., and Johnson, B.D. (1998). "Computer program CSHORE for predicting cross-shore transformation of irregular breaking waves." *Res. Rep. CACR-98-04*, Ctr. for Appl. Coast. Res., Univ. of Delaware, Newark, Del.

Kobayashi, N., Orzech, M.D., Johnson, B.D., and Herrman, M.N. (1997). "Probability modeling of surf zone and swash dynamics." *Proc., Waves '97*, ASCE, Reston, Va., 107–121.

Kobayashi, N., and Wurjanto, A. (1992). "Irregular wave setup and run-up on beaches." *J. Wtrwy., Port, Coast. and Oc. Engrg.*, ASCE, 118(4), 368–386.

Kriebel, D.L. (1994). "Swash zone wave characteristic from SUPERTANK." *Proc., 24th Coast. Engrg. Conf.*, ASCE, New York, N.Y., 2, 2207–2221.

Ochi, M.K., and Wang, W.C. (1984). "Non-Gaussian characteristics of coastal waves." *Proc., 19th Coast. Engrg. Conf.*, ASCE, New York, N.Y., 1, 516–531.

Raubenheimer, B., and Guza, R.T. (1996). "Observations and predictions of run-up." *J. Geophys. Res.*, 101(C10), 25575–25587.

Raubenheimer, B., Guza, R.T., and Elgar, S. (1996). "Wave transformation across the inner surf zone." *J. Geophys. Res.*, 101(C10), 25589–25597.

Raubenheimer, B., Guza, R.T., Elgar, S., and Kobayashi, N. (1995). "Swash on a gently sloping beach." *J. Geophys. Res.*, 100(C5), 8751–8760.

Thornton, E.B., and Guza, R.T. (1983). "Transformation of wave height distribution." *J. Geophys. Res.*, 88(C10), 5925–5938.